# Supplementary Information

## Phonon and magnon modes in preferentially oriented epitaxial α-$Fe_2O_3$ thin films investigated by Raman spectroscopy

N. Kumar*[a], I.A. Milekhin[b], Bhavana Gupta[c], Kumaraswamy Miriyala[d], V.A. Volodin[b], A.T. Kozakov[e], A.V. Nikolskii[e]

[a]Tomsk State University, 36 Lenin Ave., Tomsk, 634050 Russia.

[b]Novosibirsk State University, 1 Pirogov Ave., Novosibirsk, 630090, Russia.

[c]Department of Chemistry, School of Advanced Engineering, UPES, Dehradun, India

[d]Department of Materials Engineering, Ben-Gurion University of the Negev, Israel

[e]Research Institute of Physics, Southern Federal University, Stachki Ave. Rostov-on-Don, 344090, Russia

*E-mail: kumarphysics1975@gmail.com

## 1. Results and discussion

### 1.1. XRD analysis of α-$Fe_2O_3$ thin films deposited on $Al_2O_3$ substrates

Fig. SI-1 shows high resolution x-ray diffraction (HR-XRD) analysis of α-$Fe_2O_3$ films deposited on c- and r- plane of $Al_2O_3$ substrates. To confirm the epitaxial relation between the α-$Fe_2O_3$ layer and its underlaying substrate we performed both θ-2θ scans, which provides the information about out-of-plane alignment and off-axis ϕ-scans, which confirms the in-plane crystallographic alignment.

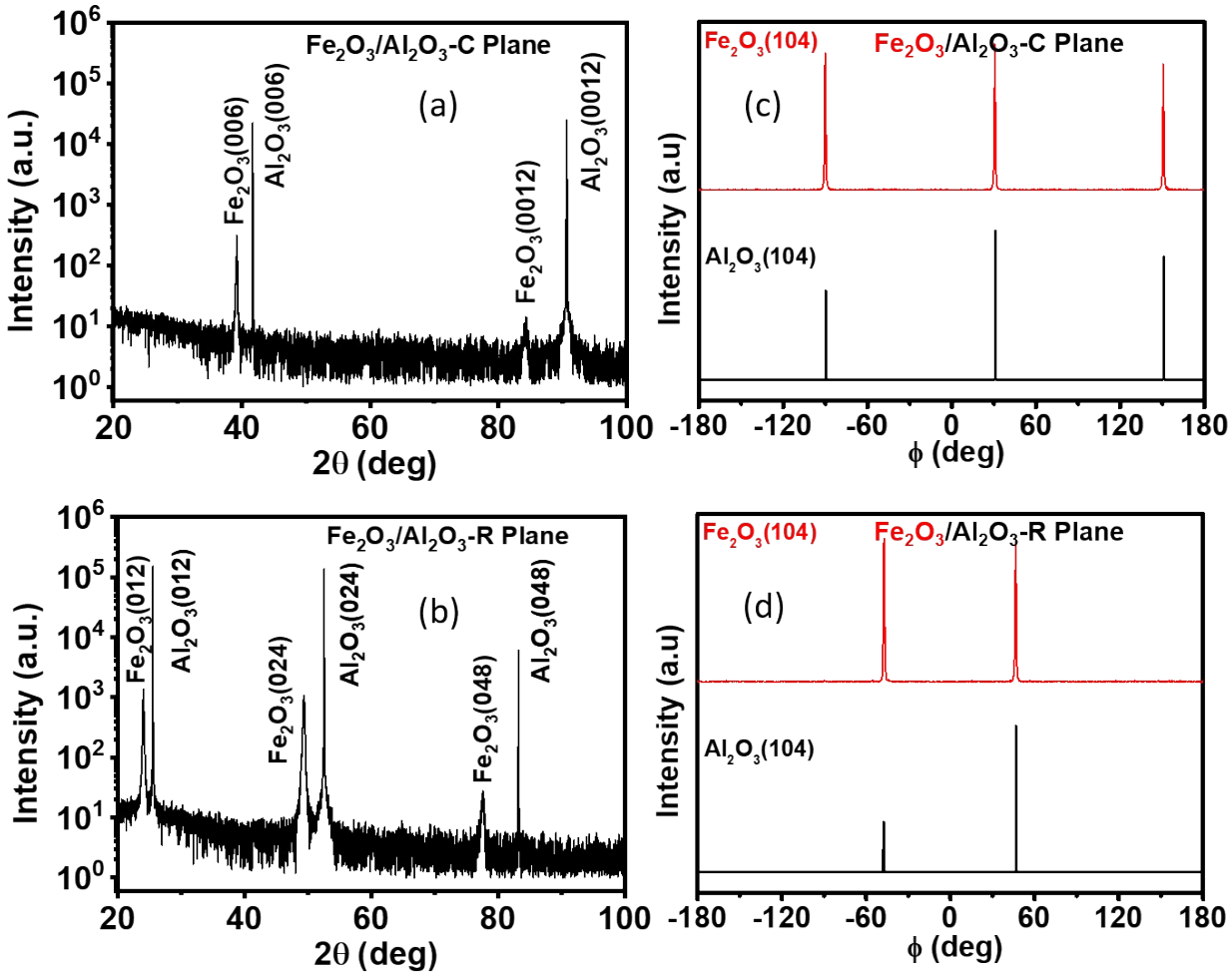


Fig. SI-1. X-ray diffraction of θ-2θ mode: (a) and (b) showed C- and R- plane oriented α-$Fe_2O_3$ film deposited on $Al_2O_3$ substrate, respectively; (c) and (d) correspond to ϕ–scans of the C- and R- plane of α-$Fe_2O_3$ film deposited on $Al_2O_3$ substrate.

Fig SI-1(a) and SI-1(b) presents the θ-2θ scans of α-$Fe_2O_3$ films deposited on C- and R-plane $Al_2O_3$ substrates respectively. The obtained diffraction pattern reveals that films are exclusively

oriented along their respective substrate orientation without any trace of other secondary orientations. The α-$Fe_2O_3$ peaks were assigned based on the ICDD file # 00-033-0664. Furthermore, the results showed good agreement with the previously reported literature.[1,2,3]

In addition, Fig. SI-1(c) and SI-1(d) shows the off axis ϕ-scans of C- and R-plane α-$Fe_2O_3$ films measured along the (104) reflection. In case of c-plane (shown in Fig. SI-1(c)), the ϕ-scan of α-$Fe_2O_3$(104) showed three distinct peaks with 120$^o$ interval which coincides with its substrate C-$Al_2O_3$(104) pattern. Similarly for R-plane α-$Fe_2O_3$, the ϕ-scan of (104) (Fig. SI-1(d)) reflection showed two distinct peaks with 90$^o$ interval, similar to its R-$Al_2O_3$(104) pattern. Thus, it is confirmed the C-plane α-$Fe_2O_3$ exhibits 3-fold symmetry, and R- plane α-$Fe_2O_3$ displays 2-fold symmetry with their corresponding substrates.[1] Finally, the combined in-plane and out-of-plane HR-XRD results confirm the heteroepitaxial growth of α-$Fe_2O_3$ film on sapphire substrate.

### 1.2. XPS analysis of α-$Fe_2O_3$ thin films deposited on $Al_2O_3$ substrates

X-ray photoelectron spectroscopy (XPS) studies were conducted on epitaxial α-$Fe_2O_3$ films grown on $Al_2O_3$ substrates in the R- and C- plane orientations. The measurements were performed using an Escalab 250 instrument with monochromated Al Kα X-ray radiation. The absolute energy resolution, determined from the full width at half maximum (FWHM) of the Ag $3d_{5/2}$ line, was 0.65 eV. All binding energies were calibrated using the C 1s line from adventitious carbon, set at a standard position of 285.0 eV. During spectral acquisition, the base vacuum pressure in the analytical chamber was maintained at $3\times10^{-10}$ mBar, and the diameter of the X-ray probe was 500 μm.

For comparative analysis, the XPS spectra of the R- and C- plane films were compared against a reference bulk $Fe_2O_3$ single crystal from a previous study.[4] Figure SI-2 presents the survey spectra for the epitaxial α-$Fe_2O_3$ films grown in the R- and C- plane, alongside the spectrum of the bulk single crystal $Fe_2O_3$. Analysis of these spectra confirms that both the bulk crystal and the two

epitaxial films oriented in R- and C- plane are of high purity, containing no elemental impurities other than iron and oxygen; the detected carbon is attributed to standard surface contamination.

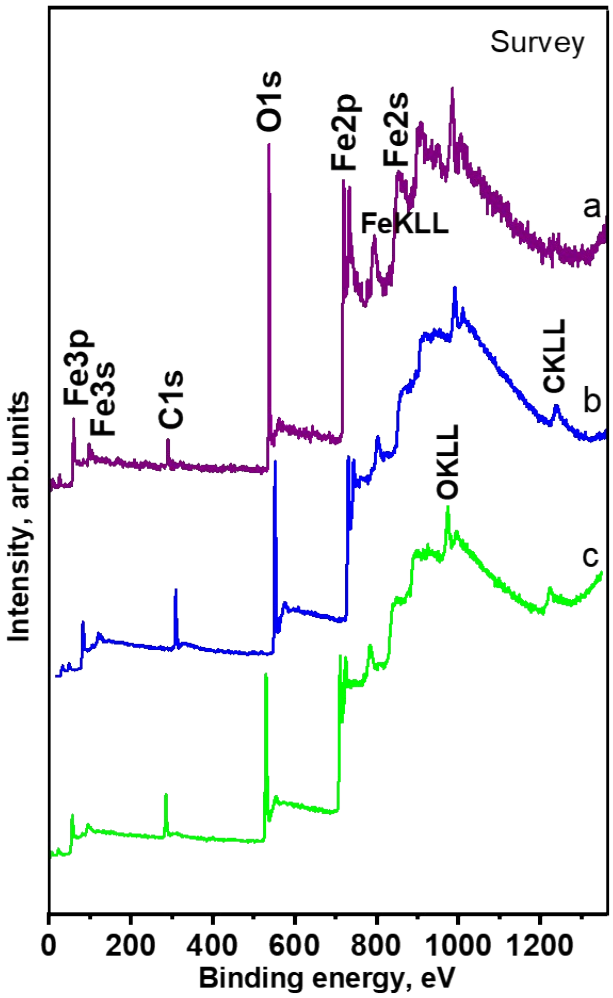


Fig. SI-2. XPS survey spectra: (a) bulk $Fe_2O_3$ single crystal; epitaxial film with orientation (b) R-plane (c) C- plane.

The Fe 2p core-level spectra for the bulk $Fe_2O_3$ crystal and the two epitaxial films oriented in R- and C- plane are shown in Fig. SI-3. The overall spectral profile of the Fe 2p spectra for both the R- and C- plane films aligns well with that of the bulk $Fe_2O_3$ crystal. As established in reference,[4] the peaks labeled A and A′ are attributed to electronic emission from the Fe $2p_{3/2}$ level, while peak C originates from the Fe $2p_{1/2}$ level. The spin-orbit splitting between these two main levels is 23.1 eV. Peaks B and D are identified as charge transfer satellites. The complex multiplet structure of the A/A′ features arise from the interaction between the core-hole vacancy on the Fe 2p level and

the 3d electrons on the iron valence orbitals. Although the overall profile is consistent, the relative intensities of these multiplet lines differ noticeably among the spectra of all three samples. The model discussed in ref. [4] does not readily explain these observed changes in multiplet intensity for the epitaxial R- and C- plane films.

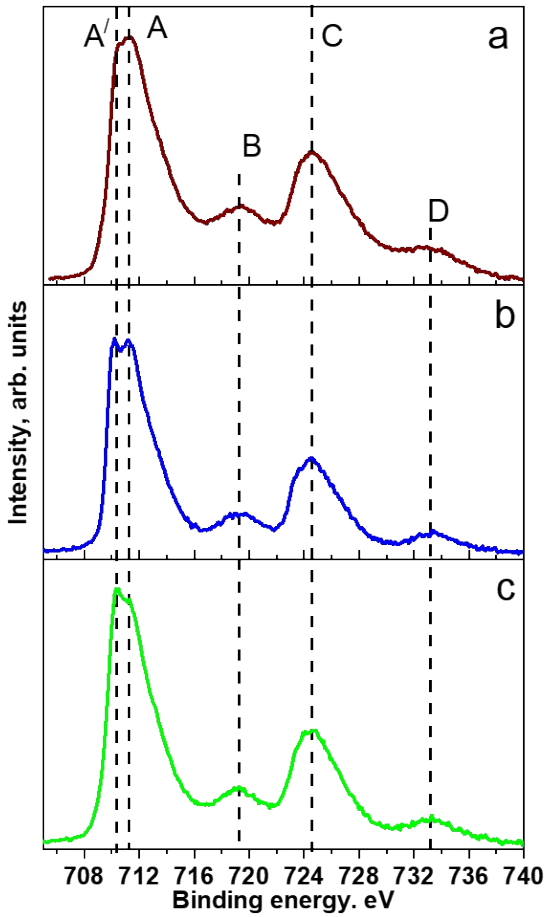


Fig. SI-3. Fe 2p XPS spectra: (a) bulk $Fe_2O_3$ single crystal; epitaxial film with orientation (b) R-plane (c) C- plane.

Figure SI-4 presents the Fe 3s XPS spectra for the bulk crystal and the epitaxial films. The primary factor governing the structure of 3s spectra in 3d transition metals is multiplet splitting in the final state of photoemission ($3s^1 3d^n$ configuration). In a single-electron approximation, this splitting results from the exchange interaction between the 3s core-hole and the unpaired electrons in the 3d subshell. In the case of LS-coupling, this interaction gives rise to two final states: a high-spin state ($^{n+2}L$), where the spin of the $3d^n$ subshell is parallel to the 3s hole spin, and a low-spin state

($^{n}$L), where it is antiparallel. Consequently, the Fe 3s spectrum typically manifests as a doublet reflecting these two states.

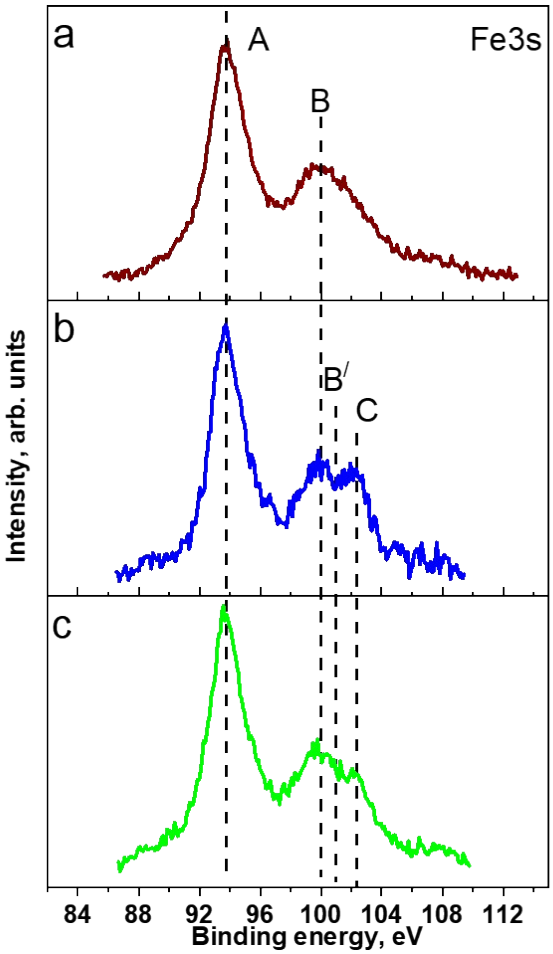


Fig. SI-4. Fe 3s XPS spectra: (a) bulk $Fe_2O_3$ single crystal; epitaxial film with orientation (b) R-plane (c) C- plane.

This simple model accurately describes the profile of the bulk $Fe_2O_3$ crystal spectrum, which is well-fitted by two components (A and B). However, the spectra of the epitaxial R- and C- plane films reveal an additional component, labeled C. The presence of this extra component indicates that the single-electron approximation is insufficient for describing these epitaxial systems. According to the data in Table SI-1, the energy separation between peaks B and A is 6.3 eV for the bulk crystal, which is consistent with trivalent iron ($Fe^{3+}$) as expected for hematite.[4]

Table SI-1. Energy position of the fine structure components of the Fe 2p and Fe 3s spectra.

| Fe 2p | | | | | Fe 3s | | | |
|---|---|---|---|---|---|---|---|---|
| A′ | A | B | C | D | A | B | B′ | C |
| 710.3 | 711.3 | 719.3 | 724.4 | 733.2 | 93.7 | 100.0 | 100.9 | 102.3 |

In contrast, for the epitaxial R- and C- plane films, the corresponding separation, if measured to the new component B′, is approximately 7.1 eV. This significant change in the multiplet splitting further underscores the necessity to modify the single-electron approximation model to correctly interpret the valence state and electronic structure of iron in these epitaxial films.

### 1.3. Polarization-resolved and temperature-dependent fitted Raman spectroscopy data

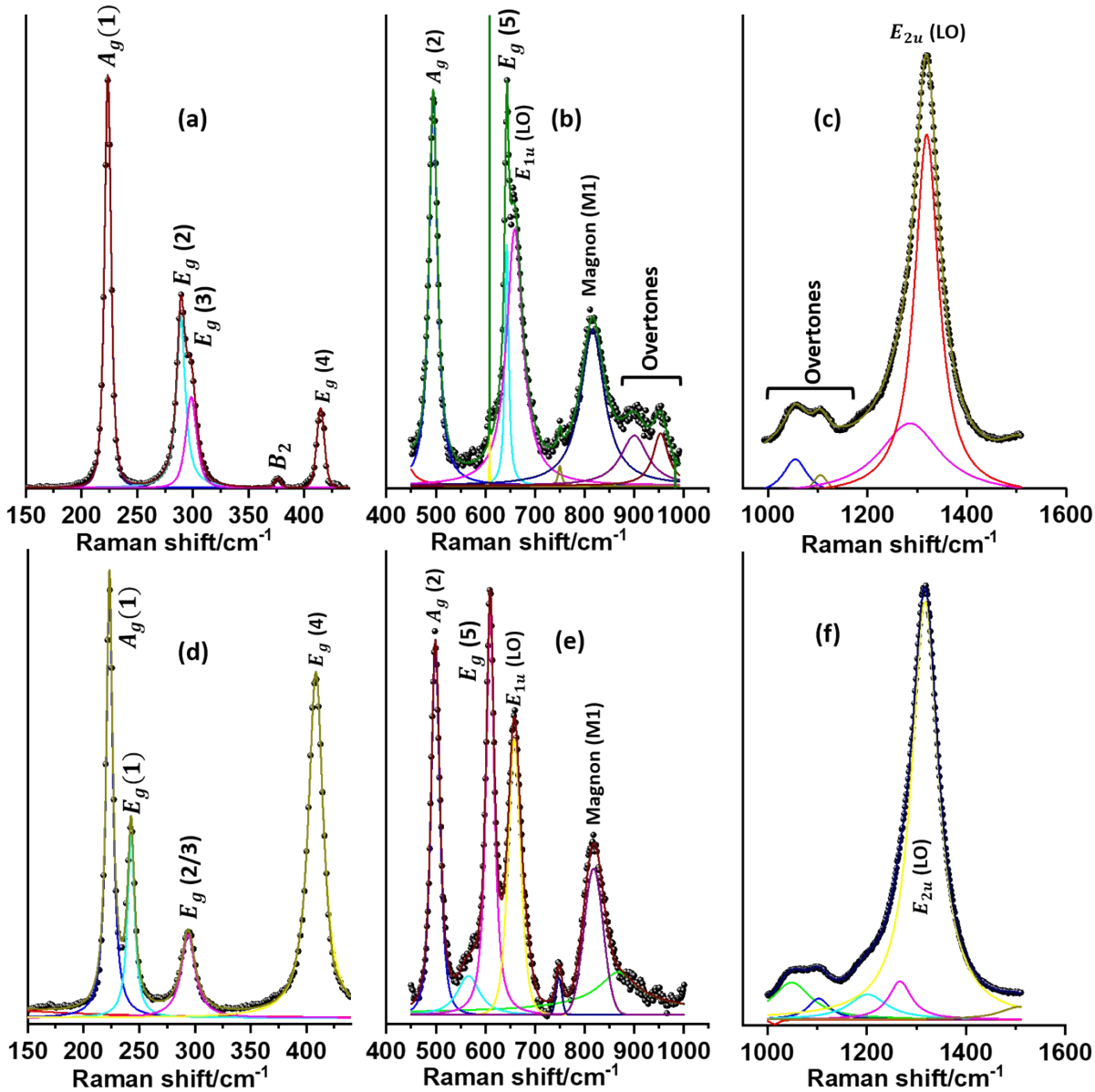


Fig. SI-5. Lorentzian fitting of Raman spectroscopy of R – plane oriented α-$Fe_2O_3$: (a), (b) and (c) at 0$^o$ polarization angle and (d), (e) and (f) 90$^o$ polarization angle in the lab frame of reference; all the other peak fitting in the polarization series is obtained by similar procedure.

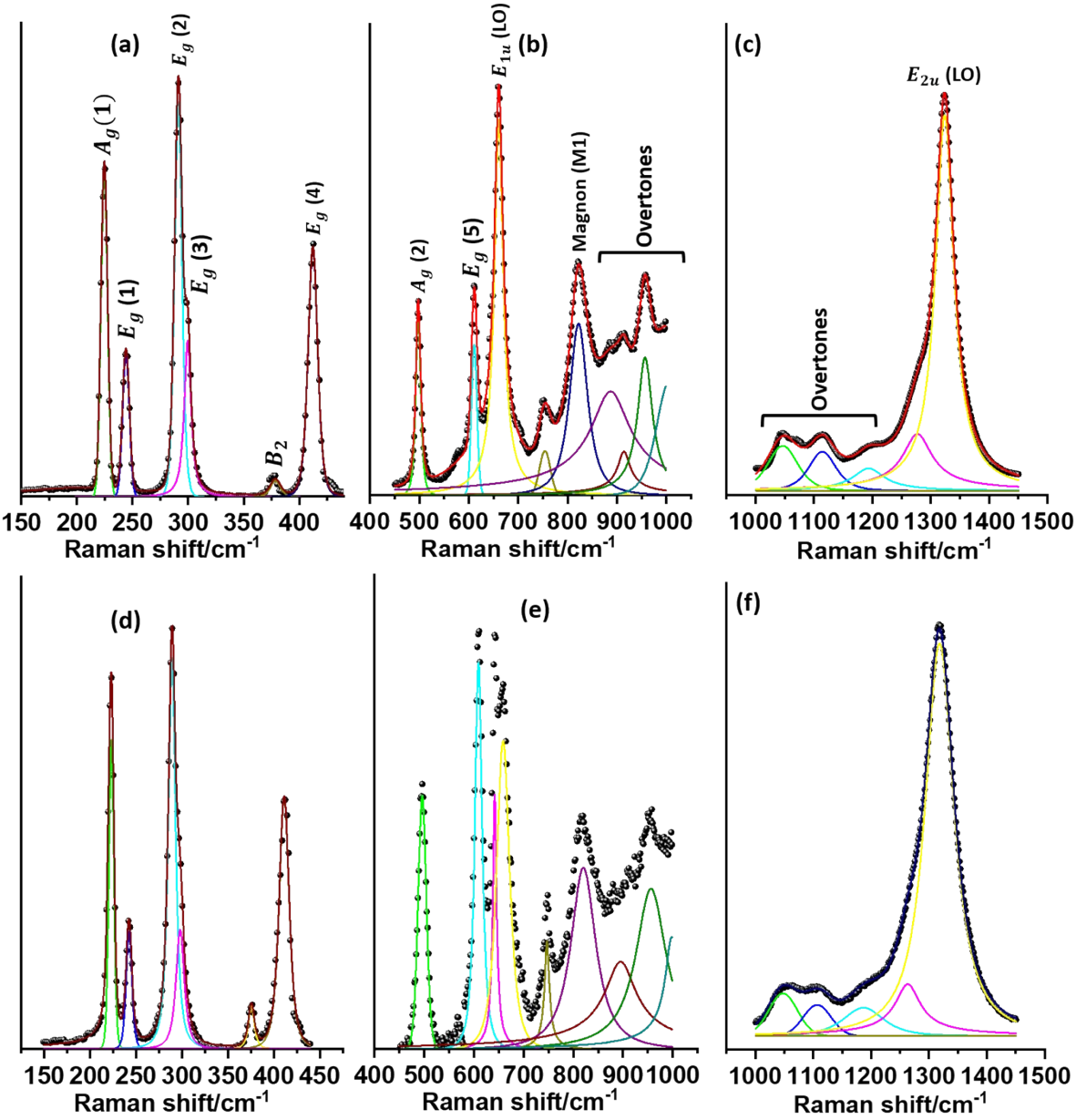


Fig. SI-6. Temperature-dependent Lorentzian fitting of Raman spectroscopy of C – plane of α-$Fe_2O_3$: (a), (b) and (c) at 75.15 K, and (d), (e) and (f) at 298.15 K; all the other peak fitting in the temperature-dependent for C – and R – planes is obtained by similar procedure.

### 1.4. Photoluminescence of α-$Fe_2O_3$ films

The photoluminescence spectra of the R- and C-plane α-$Fe_2O_3$ exhibit primary and secondary peaks at approximately 618.28 nm (~2.00 eV) and 594.1 nm (~2.08 eV), respectively, as illustrated in Fig. SI-7.

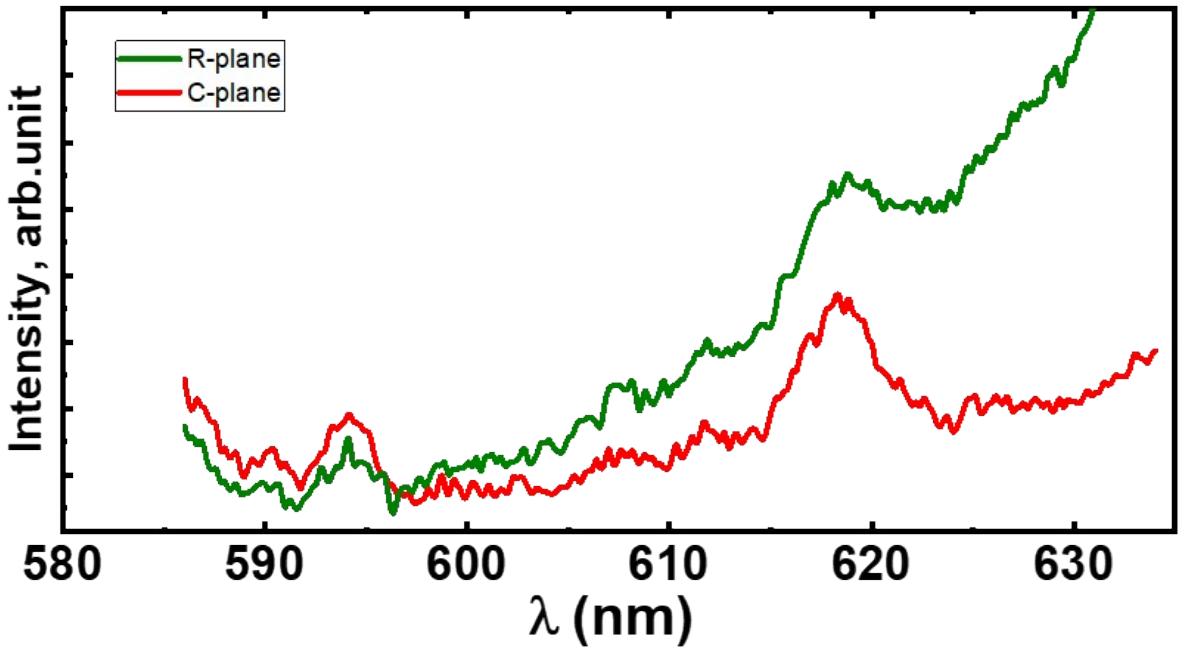


Fig. SI-7. Photoluminescence measurement of α-$Fe_2O_3$ films of R and C- oriented planes.

The primary emission arises from direct band-to-band transitions between oxygen 2p-dominated valence states and iron 3d-derived conduction bands, which corresponds to fundamental bandgap. A secondary peak appears from the formation of localized excitons, where photoexcited electrons and holes remain bound due to strong Coulomb interactions. These excitons localize primarily because of the strongly correlated Fe3d electrons and the anisotropic dielectric screening of material. The energy difference between these peaks represents the exciton binding energy, a signature of correlated electron-hole interactions. First-principles GW-BSE calculations confirm that both transitions involve electronic excitations from oxygen 2p valence states to iron 3d conduction bands.[5]

**1.5. Phonon and magnon modes investigated by Raman spectroscopy in A, R, M and C – oriented planes of α-$Fe_2O_3$ films**

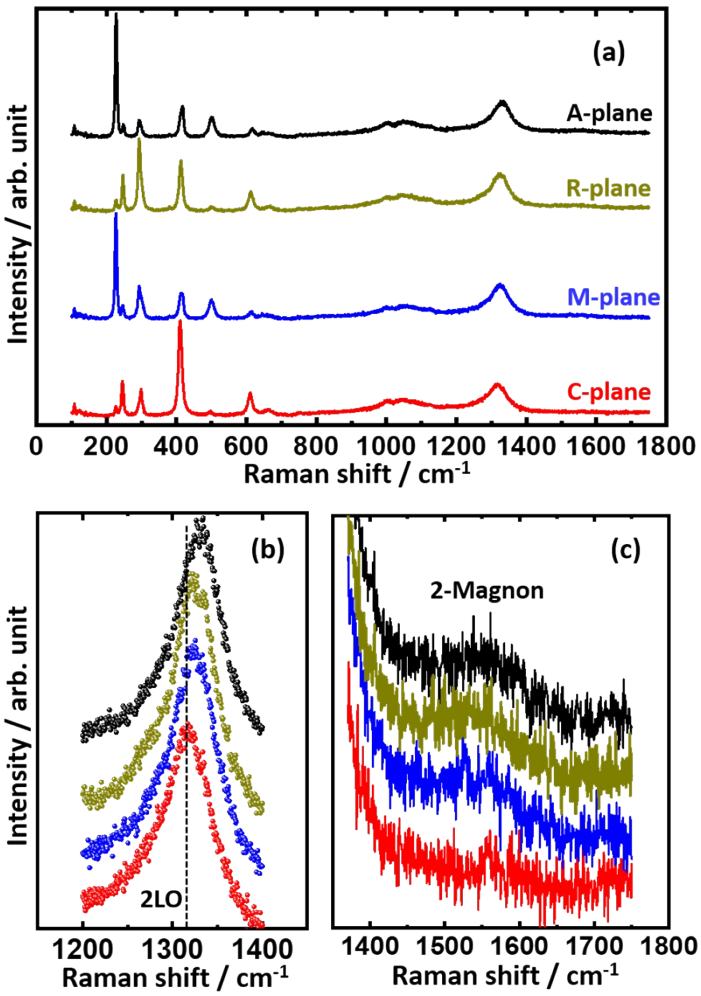


Fig. SI-8. (a) Raman spectra of α-$Fe_2O_3$ films depending upon A, R, M and C- oriented planes; (b) highlighted peak position of 2LO mode and (c) magnon mode excited in A, R, M and C- oriented planes.

**References**

1. R. Agarwal, Z. Li, K. I. Ali Khan, E. E. M. Chia and P. K. Muduli, *Phys. Rev. B: Condens. Matter Mater. Phys.,* 2024, **109**, 224408−224408.

2. D. S. Ellis, E. Weschke, A. Kay, D. A. Grave, K. D. Malviya, H. Mor, F. M. F. de Groot, H. Dotan and A. Rothschild, *Phys. Rev. B: Condens. Matter Mater. Phys.,* 2017, **96**, 094426−094432.

3. D. A. Grave, D. Klotz, A. Kay, H. Dotan, B. Gupta, I. Visoly-Fisher and A. Rothschild, *J. Phys. Chem., C* 2016, **120**, 28961–28970.

4 A. T. Kozakov, A. G. Kochur, K. A. Googlev, A. V. Nikolsky, I. P. Raevski, V. G. Smotrakov and V. V. Yeremkin, *J. Electron. Spectrosc. Relat. Phenom*., 2011, **184**, 16–23.

5. S. Piccinin, *Phys. Chem. Chem. Phys*., 2019, **21**, 2957−2967.